# Effects of the Nanomechanical Properties of Polymer Nanoparticles on Crack Patterns during Drying of Colloidal Suspensions

**Qamar Nawaz and Yahya Rharbi***

*Laboratoire de Rhéologie, UMR5520, UJF/INPG/CNRS, BP 53, Domaine Universitaire, 38041 Grenoble, France*

*Received December 16, 2007; Revised Manuscript Received June 10, 2008*

ABSTRACT: Coalescence during drying of suspensions containing glassy polymer nanoparticles generates fascinating crack patterns, whereas coalescence of soft polymer particles gives crack-free films. This process is widely used in environmental-friendly water-based coatings, which use nanosized polymer nanoparticles in the film formation process. Numerous studies have shown that polymer nanoconfinement could lead to a drastic modification of the polymer properties such as a reduction of the glass transition temperature ($T_g$). If such a change in the properties of polymers also exists when nanoconfined in nanoparticles in suspension, then one would expect an alteration in the film formation process, particularly a reduction in the minimum film formation temperature. In this paper we look at the effect of nanomechanical properties of polymer nanoparticles on crack patterns generated by particle coalescence. We study crack pattern morphology during drying of aqueous suspensions of PBMA nanoparticles (50 nm diameter) with different nanomechanical properties (different cross-linking ratios). We investigate the effect of temperature and relaxation time on crack morphologies in the transition from crack to crack-free films. These results were analyzed in terms of time−temperature superposition and compared to bulk behavior.

## 1. Introduction

Drying aqueous suspensions of polymer particles (latex) yields powder at low temperatures and homogeneous crack-free films at high temperatures. This process is of great importance in many environmental applications such as water-based coatings,[1] adhesives, and ceramic membranes for energy production. Although water-based coatings contain mainly water as the solvent, they also contain about 15% volatile organic compounds (VOCs) which aid in the fabrication of crack-free films. The ultimate objective of coating technology is to produce zero-VOC coatings.[1]

Numerous studies have been dedicated to the different phenomena involved in the film formation process, including the generation of crack patterns[6–15] and the morphology of crack-free films.[2–5] Film formation from drying of colloidal suspensions goes through three main stages[1,4,5] (Scheme 1): (a) the particles approach each other and form a closed packed array of spherical particles, (b) they deform under capillary and van der Waals forces into dodecahedron forms (12 faces), and finally (c) the polymer chains interdiffuse between adjacent particles to form a tough film.[4,5] Stage b is where the drying either yields a crack-free film or fascinating crack patterns. The minimum film formation temperature (MFFT) has its unique importance in the process of film formation, as it is the characteristic temperature where a crack-free film forms. Several groups, including Sperry et al.[18] and recently Routh et al.,[14] have investigated the MFFT for large particles using a temperature gradient bar to measure the onset temperature of film formation and related the MFFT to the glass transition temperature of bulk polymers. The MFFT is usually taken as the passage from a cloudy or cracked film to a transparent and crack-free film.[14,18]

Crack patterns during drying of colloidal suspensions of silica and hard latex have also been studied in the past decade.[6–16] Allain et al.[7] and Pouchart et al.[8] studied crack patterns in forced unidirectional drying and found an ordered array of cracks. Dufrenes et al.[10] studied the dynamics of crack propagation. Recently, Routh et al.[15] as well as Russel and Tirumkudulu[16] reported experiments on crack patterns in drying from a free surface of circular drops on solid substrates. These works suggest that capillary pressure ($P_{cap}$) acts as the motor for the initiation and propagation of cracks.[10,15,16] Negative capillary pressure acting on the two sides of an open crack is equivalent to tensile stress, which drives the crack forward.[10] The capillary stress on the fluid surface is $P_{cap} = \alpha\gamma_{a/w}/R$,[1] where $\gamma_{a/w}$ is the surface tension air/water, $R$ is the particle radius, and $\alpha$ varies between 0 and 12.9. The maximum value of the capillary stress is $P_{cap} = 12.9\gamma_{a/w}/R$.

**Scheme 1. Three Main Steps of the Film Formation Process**

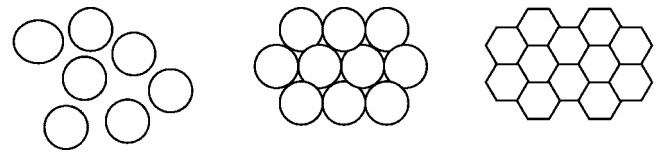

One can find in the literature two types of models to quantify crack patterns: (a) hydrodynamic and (b) mechanical. The hydrodynamic model[10,15] considers the crack patterns to result from a balance between the stress caused by capillary pressure ($P_{cap}$) and stress dissipation via water diffusion between closed packed particles. The mechanical model, proposed by Allain et al.[7] and Sasa et al.,[13] considers the film as an elastic gel and uses the stress resulting from film shrinkage during drying to evaluate the dependence of crack spacing ($\lambda_c$) on film thickness ($h$). Russell et al.[16] also developed a mechanical model based on Griffiths' criteria to predict the dependence of the $\lambda_c/h$ ratio on the residual stress above a critical value "$\sigma_{cri}$". There are other parameters that should be looked at in more detail when quantifying crack patterns and the cracking process, in particular the effect of particle nanomechanical properties (nanoconfined glass transition, relaxation spectrum, and elastic modulus) on the film cracking process. Two questions of key importance can be raised in this context: (i) What are the effects of the nanomechanical properties of nanoparticles on crack patterns and on the film formation process? (ii) Can we derive the nanomechanical properties of a single nanoconfined nanoparticle using the analysis of crack patterns?

* Corresponding author. E-mail: rharbi@ujf-grenoble.fr.

10.1021/ma7028049 CCC: $40.75 
Published on Web 07/17/2008

**Table 1. Properties of the PBMA Samples**

| | PBMA-0 | PBMA-1 | PBMA-5 | PBMA-10 |
|---|---|---|---|---|
| cross-linking (%) | 0 | 1 | 5 | 10 |
| particle size (diameter) (nm) | 68 | 50 | 46 | 52 |
| glass transition (°C) | 28 | 36 | 45 | 50 |
| elastic rubbery modulus (MPa) | 0.35 | 1 | 3.4 | 15 |

Nanoconfinement has been reported to affect the properties of many polymers.[19–30] The nanoconfined glass transition of polymers, particularly polystyrene, has been widely studied using various techniques. These results show that nanoconfined $T_g$ of polystyrene decreases with decreasing film thickness. For free-standing polystyrene films $T_g$ was found to decrease about 70 K below bulk value for 20 nm films.[20] The relaxation spectra of polystyrene, measured by the dielectric technique, were also reported to change with nanoconfinement.[22] Striking and unexplained results reported by McKenna et al.[26] on creep compliance tests reported an unusual stiffening of thin films. These changes in the properties of nanoconfined polymers could probably affect the film forming process in water-based coatings.

Most of the studies on nanoconfined polymers have been carried out on polymer thin films. Although polymers are often found nanoconfined in geometries such as spheres, less effort has been dedicated to the study of their glass transition. This information could be useful in many industrial and environmental applications such as zero-VOC coating, which uses polymer nanoparticles in the film-making process.[1] VOCs are used in coatings to lower the particle $T_g$, which permits the fabrication of crack-free films at room temperature. If the $T_g$ is reduced by decreasing the nanoparticle size, the use of VOCs could be avoided, which would have a positive impact on the environment. Recently, one report presented DSC experiments on aqueous colloidal polystyrene nanospheres in water with diameters ranging from 42 nm up to 548 nm.[30] While they found no clear shift of $T_g$ for the smallest particles they investigated (42 nm), they reported a reduction of the heat capacity ($\Delta C_p$) as the particle size is decreased.

We can divide the literature on the drying of colloidal suspensions into two groups: the first group focused on the physics of crack patterns in hard colloidal particles (Allain, Weitz, etc.),[7–16] and the second group focused mainly on the final morphology of crack-free films (Winnik, Cabane, etc.).[1–5] We are bridging together these two fields by studying the evolution of crack pattern morphology in the transition zone from the cracked regime to the crack-free film. We look at the effect of the nanomechanical properties of nanoparticles on crack patterns in the glass transition zone. We study crack patterns during drying of aqueous polymer suspensions of poly(butyl methacrylate) (PBMA) colloidal nanoparticles (50 nm diameter) with different nanomechanical properties (different cross-linking ratios).

## 2. Experimental Section

**2.1. Materials.** Monomer, butyl methacrylate (BMA, Aldrich, 99%), cross-linker, ethylene glycol dimethyl acrylate (EGDMA, Aldrich, 99%), and the surfactant sodium dodecyl sulfate (SDS, Aldrich, 99%) were used as received. The initiator, potassium persulfate (KPS, Aldrich, 98%), and sodium bicarbonate were used as received. Double deionized water was used in the emulsion polymerization.

**2.2. Synthesis.** Poly(butyl methacrylate) (PBMA) emulsions were prepared in batch emulsion polymerization using a standard emulsion polymerization setup in a 200 mL three-neck round glass flask, equipped with a mechanical stirrer, a condenser, and a nitrogen inlet. All the ingredients were mixed and heated to 70 °C except the initiator, which was added when the temperature reached the desired value. The reaction was stopped after 12 h. The cross-linker (EGDMA) was added dropwise to the mixture during polymerization in order to control the cross-linking distribution within the particles. Monomer concentration was 10 wt %, and the theoretical cross-linking fractions were 0, 1, 5, and 10%.

**2.3. Polymer and Particle Characterization.** Particle diameters ($D$) were measured using quasi-elastic light scattering (QELS) (Malvern 5000) at a 90° angle. A counting program was used for the QELS analysis. Bulk glass transition was measured by DSC (TA 2000) in modulated mode with a rate of 5 °C/min and modulation of ±1 °C/min.

Shear modulus ($G'$) measurements were carried out on AR-G2 (TA Instruments) for various frequencies and temperatures in parallel plate geometry. With these measurements, the storage shear modulus $G'$ and loss shear modulus $G''$ were calculated. All measurements were carried out in the linear viscoelastic regime in such a way that $G'$ and $G''$ were independent of the applied stress. The frequency ranged from 0.001 to 300 rad/s and the temperature from 20 to 95 °C.

Samples for rheometric measurements were prepared using PBMA powder, predried at room temperature. The PBMA powder was mixed with 10 wt % of toluene, and the samples were then compressed at 90 °C to yield 1 mm thick films. Slightly tough, crack-free films were obtained after the toluene had completely evaporated at 90 °C for more than 24 h. A thin layer (10 $\mu$m) of Lactite Superglue-3 (material: cyanoacrylate) was used to improve adhesion of the films onto the tools. The time−temperature shift factor $a_T$ from the Williams−Landed−Ferry (WLF) equation[39] was calculated using bulk $T_g$ as the reference temperature. The rubbery $G'$ values of the dry film were taken at a frequency of 1 rad/s and 95 °C. The elastic modulus $E$ of the dry film was calculated using the relation $E = 2G[1 + \nu]$, where $\nu$ is Poisson's ratio (for PBMA $\nu = 0.49$); this yields $E \approx 3G$. Because the elastic modulus of the gel evolves strongly with the drying time, the calculated $E$ values for the dry polymer films were used only as an indication for the elastic modulus of the polymer nanoparticles. A summary of the properties of the different samples used is listed in Table 1.

**2.4. Sample Preparation.** The surfactant and free ions were removed from the dispersions by a mixture of anionic and cationic exchange resins (DOWEX Marathon MR-3, Aldrich). A 0.10 ± 0.02 g aqueous suspension was gently deposited on a glass substrate (microscope slide). It formed a circular drop with a thickness of ~1 mm and a diameter of 15 mm. The glass substrate was used without pretreatment. Drying was carried out in an oven with controlled humidity and temperature. A precision measuring microbalance (METTLER TOLEDO Balance AG245) was placed inside the oven for in situ measurements of the change in mass with respect to time. The morphology of the cracks was observed with a WILD HEERBRUG MAKROSCOP Switzerland, Makrozoom 1:5, M420 1.25×, equipped with a digital camera. Thickness of the films was measured by the profilometer (SM7-ProfilTest, TL70) when the films remained adhered to the substrate. The thicknesses of the delaminated films were measured using a microscope (LEICA, DM LM) with a magnification 20×. Film thickness was taken at 3−5 mm from the edge of the circular drops and averaged over the drop circumference. The distance between cracks ($\lambda_c$) was also measured at 3−5 mm from the drop edge and averaged over all the cracks on the drop circumference to yields an average $\lambda_c$ value. Each experiment was repeated four times to yield an average value of $\lambda_c$.

## 3. Results and Discussion

**3.1. Crack Patterns in the Glassy Regime.** Water evaporation from a 15 mm circular drop on a glass substrate takes between 30 min and 48 h depending on the drying conditions. At the end of the evaporation process, a circular film of dried polymers with a thickness of ~100 $\mu$m is obtained. When the polymer suspensions were dried below their $T_g$, the cracks were well organized, longitudinal, periodic, and parallel. They emerge from the edge and propagate toward the central region (Figure 1). At room temperature, the distance between the cracks ($\lambda_c$)

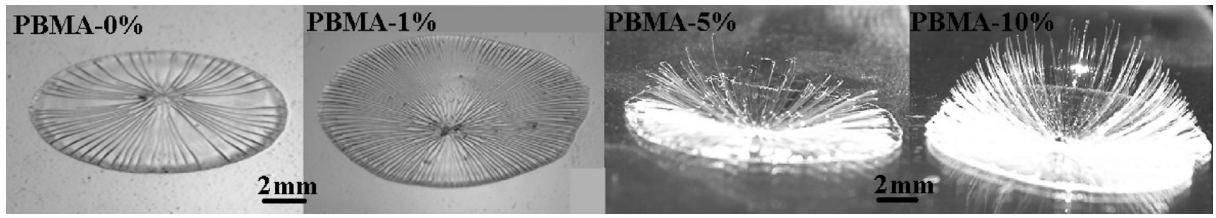


**Figure 1.** Crack patterns formed during drying of 10% PBMA colloidal suspension on glass slides at 28 °C with 20% HR. The PBMA nanoparticles are cross-linked at 0, 1, 5, and 10%.

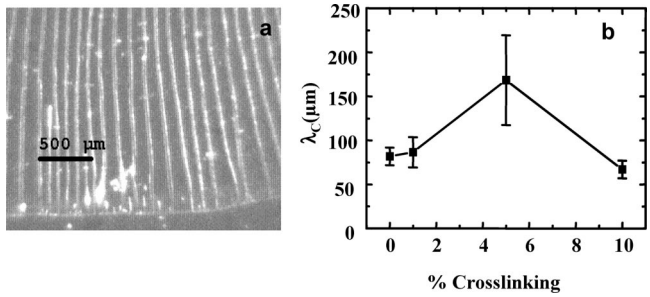


**Figure 2.** (a) Crack patterns formed during drying of (10%) PBMA colloidal suspensions cross-linked at 1%. The suspensions were dried at 23 °C in 20% humidity ratio. (b) Average distance between cracks ($\lambda_c$) in PBMA vs cross-linking ratio at 23 °C.

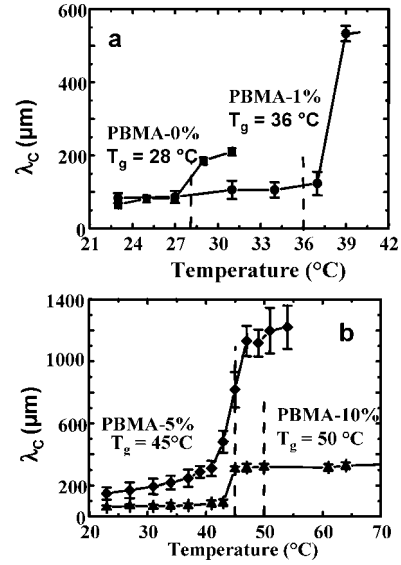


**Figure 3.** Average distance between cracks ($\lambda_c$) vs temperature during drying of colloidal PBMA suspensions (10%) at humidity ratio of 20%. The PBMA suspension have different cross-linking ratios: (a) (■) 0%, (●) 1%; (b) (◆) 5%, (▲) 10%.

was found to be 80, 85, 170, and 65 $\mu$m respectively for 0, 1, 5, and 10% cross-linking ratios (Figure 2). The $\lambda_c$ in the glassy regime is found to be in the same range for all the nanoparticles investigated here except for the 5% cross-linking particles, which shows a higher $\lambda_c$ value. This is probably due to the fact that the 5% suspension was slightly more polydispersed than the other solutions. Periodic crack patterns were observed in the forced unidirectional drying of hard colloidal suspensions between two plates by numerous groups like Allain et al.[7] and Weitz et al.[10] The films in our experiments were dried from the free surface with a circular geometry. This resulted in comparable crack patterns to the forced unidirectional drying experiments. Recently, Caddock and Hall,[8] Routh et al.,[15] Russel et al.,[16] and Chen et al.[11] also reported periodic patterns in free surface drying of circular drops of hard colloidal suspensions. It is accepted that free surface drying of small drops of liquid suspensions is heterogeneous, i.e., faster on the edges than in the center,[31] and therefore drying starts from the edges of the drop and continues toward the center.[31] This yields a unidirectional drying similar to that of the forced drying between two plates.[7−10] Cracks were reported to propagate with the drying front and to appear during the passage from the gel to the solid state.[10]

Nanoparticles with different elastic properties, i.e., different cross-linking ratios (0, 1, 5, and 10%), exhibit different arrays of cracks (Figure 1). The cracked films from the 0% and 1% cross-linked particles remained stuck to the substrates and formed periodic cracks. On the other hand, for 5% and 10% cross-linked particles, fibers formed between the cracks, disengaged from the substrate, bent, and formed a flower-like pattern (Figure 1). This flower-like pattern is more elaborate in the 10% cross-linked PBMA nanoparticles. The bending of these films enhances with increasing residual stress resulting from drying. The magnitude of film bending has been used to evaluate the stored stress during drying of colloidal suspensions.[16,17,32]

**3.2. Crack Patterns in the Glassy−Rubbery Transition.** As the drying temperature increases, the number of cracks diminishes, yet they retain their regular periodic patterns. The distance between cracks increases slowly with increasing temperature at about 2−5 $\mu$m/°C in the glassy region for all the PBMA suspensions investigated here (Figure 3). As the temperature increases, the drying rate increases, and therefore one would expect $\lambda_c$ to decrease as reported in ref 11. The increase of $\lambda_c$ with temperature in Figure 3 could be the result of drying PBMA suspensions in the glass transition zone. The increase in temperature in the glass transition zone could affect the nanomechanical properties of the particles and therefore relax part of the stress in the film, making the cracks more spaced.

A spectacular result is that the distance between cracks ($\lambda_c$) underwent an abrupt increase (5−6 times) in the proximity of the glass transition ($T_g$) within a temperature range of only 2−6 °C for all PBMA samples investigated here (Figure 3). While the cracks disappear immediately after $T_c$ ($T_c$ is the middle point temperature of the crossover) for un-cross-linked and 1% cross-linked particles, they remain apparent in medium (5%) and highly cross-linked particles (10%). For $T > T_c$, $\lambda_c$ in 5 and 10% cross-linking ratio exhibits a plateau 5−6 times higher than the $\lambda_c$ values below $T_c$. The jump temperature ($T_c$) was found to be similar to $T_g$ for 20% humidity rate for all particles investigated here (Figure 4). This plateau above $T_c$ extends up to 10 °C above $T_c$ before forming a crack-free film in the 5% cross-linked particles. On the other hand, 10% cross-linked particles do not form a crack-free film up to 23 °C above $T_c$ or $T_g$.

One attractive model to describe the periodicity of crack patterns is that a crack relaxes the stress locally, and therefore no other crack could appear within a distance $\lambda_c$ from it. The film will accumulate enough stress at a distance $\lambda_c$ from the first crack, which would generate a new crack.[7] This describes the periodic array of cracks with a period $\lambda_c$. As described above (see Introduction), two types of models were proposed to

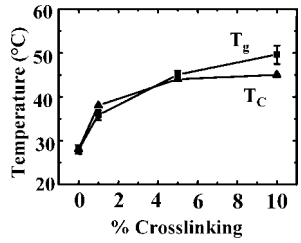


**Figure 4.** Jump temperature $T_c$ taken from the middle of the crossover zone plotted vs the cross-linking ratio and compared to the bulk glass transition ($T_g$).

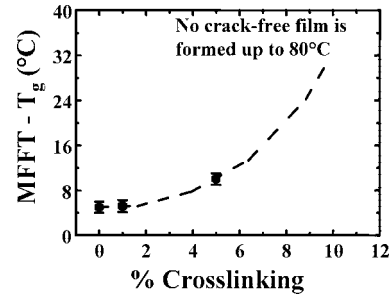


**Figure 5.** Minimum film formation temperature MFFT compared to $T_g$ for various cross-linking ratios. No crack-free film is obtained for PBMA-10% up to a temperature of 80 °C.

describe the driving forces for crack patterns. The first one is a mechanical model,[7,13] and the second is hydrodynamic.[10,15] The mechanical model treats the colloidal gel as an elastic medium and predicts that the cracks would appear if the elastic stress exceeds a critical value ($\sigma_{cri}$). This model could predict the dependence of $\lambda_c$ on the film thickness. The hydrodynamic model[15] attributes the crack patterns to tensile stresses resulting from negative capillary pressure ($P_{cap}$) and the energy dissipation to the diffusion of water between closed packed particles. There are other parameters that should be looked at in more detail when quantifying crack patterns and the cracking process, in particular the effect of particle nanomechanical properties. The rapid jump of $\lambda_c$ in the trans-$T_g$ region cannot be well explained except by a rapid change in the nanomechanical properties of the particles. In this transition the particles go from a glassy to a rubbery state. As the particles go into the rubbery regime, part of the capillary stress dissipates through viscous relaxation via particle deformation, which yields an increase in $\lambda_c$. This explanation is supported by the similarity between the variation trend of the jump temperature ($T_c$) and $T_g$ (Figure 4).

It is well accepted that the tensile stress that causes films to crack results from capillary pressure $P_{cap}$. The maximum value of $P_{cap}$ is ~13.5 MPa for our system. Part of this stress relaxes during drying due to (a) friction between particles and gel compaction and (b) viscous dissipation of the stress via deformation of the nanoparticles. If the residual stress exceeds a threshold value, the gel cracks before a crack-free film can be formed. Russel and Tirumkudulu[16] proposed that $\lambda_c/h$ ($h$ = film thickness) depends on the residual stress ($\sigma$) above the critical stress value for the initiation of an individual crack ($\sigma_{cri}$). They proposed that $1/K^{3/2} \approx f(\lambda_c/h)$, with $K = \sigma/\sigma_{cri}$. Though this model was proposed for glassy particles, we will use it to qualitatively describe crack patterns in the transition from glassy to rubbery regimes. One can imagine that in the short temperature range across $T_c$ the hydrodynamic parameters are constant (film thickness, drying rate, etc.), and only the residual stress in the gel ($\sigma$) decreases across $T_g$ from $\sigma_{glassy}$ in the glassy regime to $\sigma_{ruberry}$ in the rubbery regime.

In our experimental conditions the gel always cracks in the glassy regime below $T_c$, which infers that $\sigma_{glassy} > \sigma_{cri}$. There are two situations for the rubbery regime above $T_c$: (1) If $\sigma_{rubbery}$ falls below $\sigma_{cri}$ ($\sigma_{rubbery} < \sigma_{cri}$), a crack-free film is obtained, which is the case in the low cross-linking ratio, in which the rubbery elastic modulus $E < 1$ MPa. (2) If $\sigma_{rubbery}$ falls below $\sigma_{glassy}$ but is still higher than $\sigma_{cri}$, ($\sigma_{glassy} > \sigma_{rubbery} > \sigma_{cri}$), then crack patterns are generated with larger $\lambda_c$ values than those obtained in the glassy regime. This is probably the case for the 5% and 10% cross-linking nanoparticles, which exhibit a rubbery elastic modulus $E > 3.4$ MPa. The rapid change in $\lambda_c$ vs temperature depicts the relaxation of the residual stress via viscous dissipation within the nanoparticles. Relaxation of the viscous stress in un-cross-linked and low cross-linked particles ($E < 1$ MPa) generates crack-free films immediately above $T_c$. However, because high cross-linked particles (10%) exhibit a high rubbery elastic modulus $E \approx 15$ MPa, a cracked film is obtained above $T_c$ with a $\lambda_c$ value 5−6 times higher than $\lambda_c$ in the glassy regime. We can conclude that the magnitude of the change in $\lambda_c$ is the signature of the magnitude of change in the stress within the nanoparticles.

In terms of the hydrodynamic model, one would expect that as the particles deform, the size of the interstices between them shrinks, which would reduce the diffusion of water in the film and consequently lead to a reduction of $\lambda_c$. This mechanism should be taken into consideration for a qualitative evaluation of the residual stress variation in the $T_c$ zone. In the following we will exploit only the temperature $T_c$ and the time corresponding to it ($\tau_c$) to monitor the change in the particle properties.

**3.3. Minimum Film Formation Temperature (MFFT).** The MFFT is an important parameter in the film formation process in the coating industry. It defines the onset temperature for crack-free film formation. Traditionally, MFFT is measured by drying suspensions on a temperature gradient bar, and the MFFT is taken as the onset temperature where the film goes from cloudy and cracked to transparent. The results shown in Figure 5 question the definition of the MFFT. In Figure 5, we compare the MFFT to $T_g$ for drying humidity of 20%. MFFT is about 5 °C higher than $T_g$ for an un-cross-linked sample. As the cross-linking ratio increases, the difference between MFFT and $T_g$ increases. Highly elastic particles (10% cross-linked) go from stages of narrower cracks to more spaced cracks, without reaching the crack-free film. Un-cross-linked and 1% cross-linked particles go directly from cracked to crack-free films (Figure 3). This proves that the $T_c$ and MFFT are two different parameters for describing the film formation process. While $T_c$ is related to the relaxation of the stress during the transition from glassy to rubbery, the MFFT is linked to closure of the interstices between particles. Sperry et al.[18] and recently Routh et al.[14] have investigated the variation of MFFT (measured in a temperature gradient bar) with drying time and found that in many cases MFFT decreases below bulk $T_g$ with a decreasing drying rate for large particles (>170 nm). They compared the variation of MFFT with the WLF equation and extrapolated a bulk $T_g$ value.

Routh and Russel[2] summarized the various possible mechanisms for particle deformation during particle coalescence in a single model and predicted the particle coalescence at different times and temperatures. Various mechanisms are possible for particle coalescence: wet sintering at a high temperature, capillary sintering close to $T_g$, and dry sintering below glass transition. This type of model can predict the temperature and time for interstice closure ($t_{clos}$) and consequently MFFT. Interstice closure during drying could be manifested in large particles by the disappearance of both cracks and film cloudiness. The variation of $t_{clos}$ on temperature also depends on the drying rate and on sintering mechanisms. Defrenes et al.[10] have

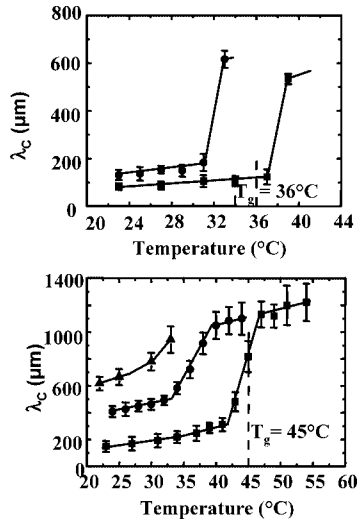


**Figure 6.** (a) Crack evolution at different humidity ratios during drying of PBMA cross-linked at 1%: HR 45% (●) and HR 20% (■). (b) Crack evolution at different humidity ratios during drying of 5% cross-linked PBMA: HR 20% (■), HR 45% (●), and HR 80% (▲).

shown that cracks occur during the passage from gel to solid and are generated mainly by capillary stress (capillary sintering).

**3.4. Effects of Drying Time.** Stress relaxation is an important factor in crack generation; the more time given to relax the stress in the gel, the less likely cracks will generate. In order to monitor the effect of stress relaxation on crack patterns, we studied crack formation for different drying times. The relaxation time was monitored by varying the drying time via controlling the humidity ratios (HR). The total drying time was taken as the time which yields a solid content of 98%. The drying time increased with increasing the humidity ratio and decreasing the temperature from 30 min at 43 °C, HR 20% to 2 days at 24 °C, HR 80%.

The overall morphology of crack patterns remains periodic for all drying times investigated, with some variations: the distance between cracks increases as the drying time increases for the same temperature. The fibers in the 5% cross-linking ratio do not bend and remain stuck to the substrate for HR 45% and HR 80%. Figure 6 depicts the distance between cracks ($\lambda_c$) vs temperature for various drying conditions. As the drying time increases, the general dependence of $\lambda_c$ on temperature is the same for all drying times investigated here; $\lambda_c$ increases slowly at low temperatures and undergoes a rapid increase at a temperature $T_c$. While $\lambda_c$ exhibits a plateau in 5% cross-linked particles above $T_c$, cracks disappear immediately above $T_c$ for the 1% cross-linked particles. The 1% cross-linked curve and the corresponding $T_c$ values shift about 6 °C to lower temperatures for drying times going up from 40 min to 1.5 h. The $\lambda_c$ curve and $T_c$ in 5% cross-linked particles shift about 8 and 15 °C when the drying time increases by about 1.5 and 30 h, respectively.

Many studies[11,12] have shown that increasing drying time yields a steady increase in the distance between cracks for hard particles. This was also the case for this system below $T_c$, where the whole plot of $\lambda_c$ vs temperature shifts up in the *y*-axis (Figure 6). The jump of $\lambda_c$ at $T_c$ in Figure 6 represents the changes in polymer nanomechanical properties, which probably represent the stress relaxation in the gel via viscous dissipation within the nanoparticles. If this stress relaxation at $T_c$ for a time $\tau_c$ is linked to polymer relaxation in the nanoparticles, it should obey the time−temperature superposition concepts. One can identify two possibilities to explain the change of $T_c$ with the drying time: (a) the $T_g$ of the nanoparticles is unaffected by nanoconfinement and is equal to that of bulk, and (b) $T_g$ shifts to a lower temperature because of nanoconfinement. The pair $\tau_c$, $T_c$ are plotted using the Angell representation and fitted to the Vogel−Fulcher−Tamman (VFT) model:[33]

$$\tau = \tau_0 e^{-B/(T-T_0)} \quad (1)$$

where $B$ is the activation energy and $T_0$ is the temperature at which the relaxation times $\tau$ diverges. In Figure 7, we show the Angell representation of $\ln(\tau_c/\tau_c(T_g))$ vs $T_g/T_c$. $T_g$ is the bulk glass transition, and $\tau_c(T_g)$ is the time corresponding to the jump zone for the low-humidity condition, which yields $T_c \approx T_g$. The $\tau_c$ and $T_c$ are compared to the temperature shift factor $a_T$ calculated from the shear storage modulus ($G'$) data in Figure 8. The two plots follow different tendencies, inferring that the $T_0$ and the activation energy ($E_{acti}$) values of 50 nm PBMA nanoparticles are different from those of bulk. We checked whether nanoconfined glass transition is reduced below bulk value by comparing the experimental data to the VFT model using a bulk activation energy from the rheometry results ($E_{acti}$ = 48 kJ/mol) and various $T_0$ values. As $T_0$ decreases below bulk value (178 K), the VFT model approaches the experimental results (Figure 8), which infers that $T_0$ for PBMA nanoparticles is more compatible with a value 20 K lower than that of bulk. Because the characteristic temperature $T_c$ is equal to the bulk $T_g$ for all the particles investigated here for low drying time (~2000 s), we cannot draw the conclusion that nanoconfined glass transition of these nanoparticles decreases by 20 K below bulk value.

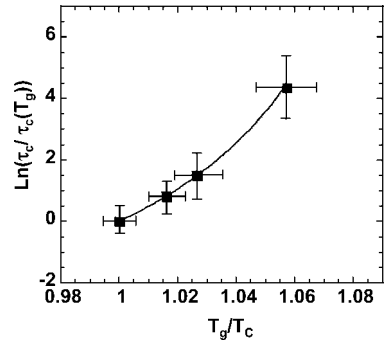


**Figure 7.** Angell plot of the jump time $\tau_c$ vs the corresponding temperature $T_c$, $\ln(\tau_c/\tau_c(T_g))$ vs $T_g/T_c$, for 5% cross-linked PBMA suspensions, dried at various humidity ratios and temperatures.

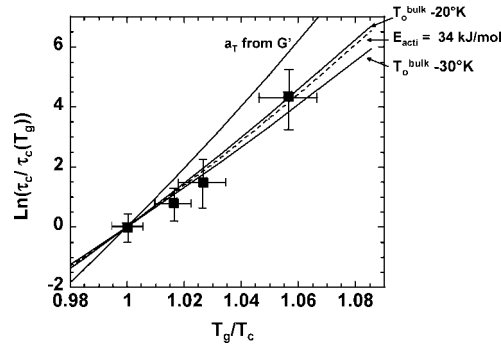


**Figure 8.** Plot of $\ln(\tau_c/\tau_c(T_g))$ vs $T_g/T_c$ for 5% cross-linked PBMA, compared to the shift factor for the shear storage modulus $G'$, $\ln(a_T)$ vs $T_g/T$, for 5% cross-linked PBMA (straight line). The shift factor $a_T$ is calculated from the storage modulus $G'$ curves, measured in the shear experiment on the bulk polymer (see Experimental Section). The $\ln(a_T)$ fits to the VFT model with $T_0$ = 178 K and an activation energy of $E_{acti}$ = 48 kJ/mol. The experimental curves are compared to the VFT model using the bulk activation energy (48 kJ/mol) and a lower $T_0$ value (straight lines, $T_0$ − 20 K and $T_0$ − 30 K). The dashed curve: the VFT model using bulk value of $T_0$ and an activation energy of 30 kJ/mol.

In many situations, nanoconfinement has been found to affect the glass transition of nanoconfined polymers.[19–30] Polystyrene free-standing ultrathin films were found to exhibit a $T_g$ reduction of 70 K when film thickness is in the order of 20 nm.[20] $T_g$ in acrylate polymers (PMMA and PiBMA) were found to exhibit a weaker dependence (at the most 8 K) on film thickness.[35] It is well accepted that the reduction of $T_g$ is the result of higher mobility at the surface with respect to bulk, and therefore the reduction of $T_g$ is a function of the surface-to-volume ratio. Nanospheres have a surface-to-volume ratio 6 times higher than that of supported films and 3 times that of free-standing films. A 50 nm diameter nanoparticle has the same surface-to-volume ratio as a supported film of 8.3 nm. However, Ediger et al.[30] using DSC measurements on colloidal suspensions of polystyrene nanoparticles did not see any shift in bulk $T_g$ for particles as small as 42 nm. On the other hand, they observed a reduction of $\Delta C_p$ and suggested that a mobile part of the polymer is not accessible in their DSC experiment, and they analyzed the reduction of $\Delta C_p$ in terms of a mobile layer surface. Herminghaus et al.[37] using solid NMR also suggested that the presence of a mobile layer at the surface of polystyrene nanoparticles. Reference 38 showed that the $T_g$ of polystyrene nanoparticles dispersed in nanoblends decreases with decreasing particle diameter.

The same results were also compared to the VFT model using bulk $T_0$ value (178 K) and various activation energies. In terms of this model, we found the activation energy $E_{acti}$ to be lower than that of bulk ~34 kJ. These analyses assume no variation in the shape of the relaxation spectra with temperature and nanoconfinement. Figure 6b shows that $\lambda_c$ variation with temperature broadens as the temperature decreases below bulk $T_g$. This might infer that the relaxation spectrum of these nanoparticles also broadens in the glassy regime. Dielectric relaxation experiments on PS and PMMA ultrathin films were analyzed either in terms of a shift in the glass transition[22] or broadening in the relaxation spectrum in the proximity of glass transition. The activation energy was reported to increase with film thickness.[22] There might be a combination of possible mechanisms that could explain the deviation from bulk behavior: (1) a lower magnitude of nanoconfined $T_g$ reduction, (2) the relaxation spectrum broadens below glass transition, and (3) the activation energy of nanoparticles is different from that of bulk. Another mechanism worth mentioning is the effect of plasticizing on nanoconfined $T_g$. Torkelson et al.[36] have reported results where plasticizers inhibit $T_g$ reduction in nanoconfined thin films. Water could act as a plasticizer for PBMA nanoparticles, which according to refs 28 and 36 might inhibit $T_g$ reduction.

If we believe that the rapid jump in $\lambda_c$ is mainly related to stress relaxation in the nanoparticle, then one could conclude that cross-linked PBMA nanoparticles behave differently from bulk below glass transition. However, we cannot clearly conclude that nanoconfined glass transition of the 50 nm cross-linked PBMA is reduced by 20 K below bulk $T_g$.

## 4. Conclusions

In this work we have investigated the diversity of crack patterns formed by drying 50 nm PBMA nanoparticle suspensions at different temperatures. As the temperature increases, three possible crack patterns can be obtained: (1) Below the glass transition temperature, the distance between cracks ($\lambda_c$) increases slightly. (2) The $\lambda_c$ exhibits a rapid jump at a temperature $T_c$, suggesting a prompt change in the nanomechanical properties (stress relaxation) of the polymer nanoparticles. (3) $\lambda_c$ exhibits a plateau before a crack-free film is obtained. At a high drying rate the jump temperature $T_c$ was found to be similar to bulk $T_g$. As the drying time increases, $T_c$ shifts to lower temperatures. These changes in crack patterns with time and temperature were analyzed in terms of the time−temperature superposition concept and compared to the rheometry data for bulk polymers. The Angell plot of temperature ($T_c$) and the time ($\tau_c$) corresponding to the abrupt change in $\lambda_c$ were found to be different from rheometry data for bulk, which infers that the nanomechanical properties of the 50 nm cross-linked nanoparticles deviate from bulk behavior.

## References and Notes


(1) Steward, P. A.; Hearn, J.; Wilkinson, W. C. *Adv. Colloid Interface Sci.* **2000**, *86*, 195.
(2) Russel, W. B.; Routh, A. F. *Langmuir* **1999**, *15*, 7762.
(3) Rharbi, Y.; Boué, F.; Joanicot, M.; Cabane, B. *Macromolecules* **1996**, *29*, 4346; *Europhys. Lett.* **1999**, *46*, 472.
(4) Feng, J.; Winnik, M. A.; Shivers, R. R.; Clubb, B. *Macromolecules* **1995**, *28*, 7671.
(5) Cabane, B.; Chevalier, Y.; Pichot, C.; GraiIlal, C.; Joanicot, M.; Wong, K.; Maquet, J.; Lindner, P. *Colloid Polym. Sci.* **1992**, *270*, 806.
(6) Brinker, C. J.; Scherer, G. W. *Sol-Gel Science*; Academic Press: San Diego, 1990.
(7) Allain, C.; Limat, L. *Phys. Rev. Lett.* **1995**, *74*, 2981.
(8) Hull, D.; Caddock, B. D. *J. Mater. Sci.* **2002**, *37*, 825.
(9) Pauchard, L.; Adda-Bedia, M.; Allain, C.; Couder, Y. *Phys. Rev. E* **2003**, *67*, 027103–1.
(10) Dufresne, E. R.; Crowin, E. I.; Greenblatt, N. A.; Ashmore, J.; Wang, D. Y.; Dinsmore, A. D.; Cheng, J. X.; Xie, X. S.; Hutchinson, J. W.; Weitz, D. A. *Phys. Rev. Lett.* **2003**, *91*, 224501-1.
(11) Chen, K.; Taflove, A.; Kim, Y. L.; Backman, V. *Appl. Phys. Lett.* **2005**, *86*, 033101-1.
(12) Kitsunezaki, S. *Phys. Rev. E* **1999**, *60*, 6449.
(13) Komatsu, T. S.; Sasa, S. *Jpn. J. Appl. Phys.* **1997**, *36*, 391.
(14) Lee, W. P.; Routh, A. F. *JCT Res.* **2006**, *3*, 301.
(15) Lee, W. P.; Routh, A. F. *Langmuir* **2004**, *20*, 9885.
(16) Tirumkudulu, M. S.; Russel, W. B. *Langmuir* **2005**, *21*, 4938.
(17) Tirumkudulu, M. S.; Russel, W. B. *Langmuir* **2004**, *20*, 2947.
(18) Sperry, P. R.; Snyder, B. S.; O'Dowd, M. L.; Lesko, P. M. *Langmuir* **1994**, *10*, 2619.
(19) Reiter, G. *Europhys. Lett.* **1993**, *23*, 579.
(20) Forrest, J. A.; Dalnoki-Veress, K.; Stevens, J. R.; Dutcher, J. R. *Phys. Rev. Lett.* **1996**, *77*, 2002.
(21) Keddie, J. L.; Jones, R. A. L.; Cory, R. A. *Europhys. Lett.* **1994**, *27*, 59.
(22) Fukao, K.; Miyamoto, Y. *Phys. Rev. E* **2000**, *61*, 1743.
(23) Kawana, S.; Jones, R. A. L. *Phys. Rev. E* **2001**, *63*, 021501.
(24) DeMaggio, G. B.; et al. *Phys. Rev. Lett.* **1997**, *78*, 1524.
(25) Ellison, C. J.; Torkelson, J. M. *Nat. Mater.* **2003**, *2*, 695.
(26) O'Connell, P. A.; McKenna, G. B. *Eur. Phys. J. E* **2006**, *20*, 143.
(27) Varnik, F.; Baschnagel, J.; Binder, K. *Phys. Rev. E* **2002**, *65*, 021507.
(28) Riggleman, R. A.; Yoshimoto, K.; Douglas, J. F.; dePablo, J. J. *Phys. Rev. Lett.* **2006**, *97*, 045502.
(29) Alcoutlabi, M.; McKenna, G. B. *J. Phys.: Condens. Matter* **2005**, *17*, 461.
(30) Sasaki, T.; et al. *J. Chem. Phys.* **2003**, *119*, 8730.
(31) Deegan, R. D.; Bakajin, O.; Dupont, T. F.; Huber, G.; Nagel, S. R.; Witten, T. A. *Nature (London)* **1997**, *389*, 827.
(32) Martinez, C. J.; Lewis, J. A. *Langmuir* **2002**, *18*, 4689.
(33) Angell, C. A. *Science* **1995**, *267*, 1924.
(34) Wind, M.; Graf, R.; Heuer, A.; Spiess, H. W. *Phys. Rev. Lett.* **2006**, *91*, 155702–1.
(35) Ellison, C J; Kim, S. D.; Hall, D. B.; Torkelson, J. M. *Eur. Phys. J. E* **2002**, *8*, 155.
(36) Ellison, C. J.; Ruszkowski, R. L.; Fredin, N. J.; Torkelson, J. M. *Phys. Rev. Lett.* **2004**, *92*, 095702.
(37) Herminghaus, S.; Seemann, R; Landfester, K. *Phys. Rev. Lett.* **2004**, *93*, 017801.
(38) Rharbi, Y. *Phys. Rev. E* **2008**, *77*, 031806.
(39) Ferry, J. D. *Viscoelastic Properties of Polymers*; John Wiley and Sons: New York, 1961.


MA7028049